Article

Rapid Identification and Quantification of Microplastics in the Environment by Quantum Cascade Laser-Based Hyperspectral Infrared Chemical Imaging

Sebastian Primpke,* Matthias Godejohann, and Gunnar Gerdts

Cite This: *Environ. Sci. Technol.* 2020, 54, 15893−15903

Read Online

ACCESS | Metrics & More | Article Recommendations | Supporting Information

ABSTRACT: The monitoring of the emerging contaminant, microplastics, in the environment, in water supply, and for food safety is of major interest to science, consumers, and governments. While the chemical analysis of these particles is considered mandatory, a rapid and reliable method for the determination of particle sizes, shapes, and numbers is missing, as existing methods are not fitting into current laboratory measurement routines. In this study, we present an approach for circumventing these issues through the application of quantum cascade laser-based microscopy combined with an automated data analysis. This method allows the measurement of an area of 144 mm^2 in 36 min, with a pixel resolution of 4.2 μm, which is an appropriate timeframe and spatial resolution for routine measurements. The performance was compared to the existing state-of-the-art Fourier transform infrared microscopy analyses. Further, the application of the method on various environmental samples was investigated to examine its capacity to provide number and variety of present particles. The described analytical procedure overcomes the last restrictions for schedulable and rapid microplastic monitoring, resulting in a highly detailed data set for particle numbers, particle shapes, and polymer types.
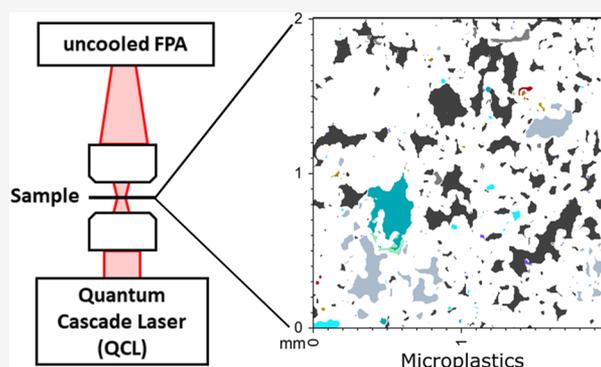
INTRODUCTION

Quantifiying the presence of microplastics (MPs) in the environment is of high importance for science, consumers, and governments.[1,2] These particles accumulate over time in the environment and pose potential risks to humans due to their sizes, polymer backbones, and chemical additives.[3] Furthermore, they can act as transport vectors for chemical and microbial contaminants.[4] While MPs have been found even in the remotest areas of the world,[5−10] systematic and widespread monitoring, especially down to small sizes of only a few micrometers, is still missing.[2,11] These small particles exhibit the highest potential to cause harm, as they can be easily consumed by organisms.[12] To better understand the potential risks, it is highly desirable to identify and quantify these particles together with their chemical compositions and size distributions.[3]

Chemical and physical characteristics of MPs are investigated using various analytical techniques such as Fourier transform infrared microscopy (μFT-IR)[13−15] or Raman microscopy[16,17] to identify particle compositions, numbers, and sizes.[18−20] Complementary to these techniques, thermal degradation coupled with gas chromatography−mass spectrometry[21,22] is applied to identify the present polymers and determine masses. The low throughput of these methods, with measurement times ranging from a few hours (FT-IR and

thermal degradation) to days (Raman), prevents their common application for routine environmental monitoring.[11,19]

To overcome this limitation, the speed of hyperspectral imaging via microbolometers here working as focal plane arrays (FPAs) can be combined with high brilliance infrared sources based on broadly tunable external cavity quantum cascade lasers (EC-QCLs). With such systems, it is possible to perform measurements in a much larger field of view with 14 times more pixel per measurement field compared to the existing state-of-the-art FT-IR microscopy techniques. Such systems were already used for the label-free automated histopathology of cancerous tissues[23] and the insertion of known MP (target analysis) into cells.[24] Nevertheless, it was not tested previously for the analysis of unknown MP (nontarget analysis) in environmental samples, like sediment,[9] snow,[8] or marine surface water samples,[25] using a bright IR light source in combination with the ability to collect mosaics of hyperspectral
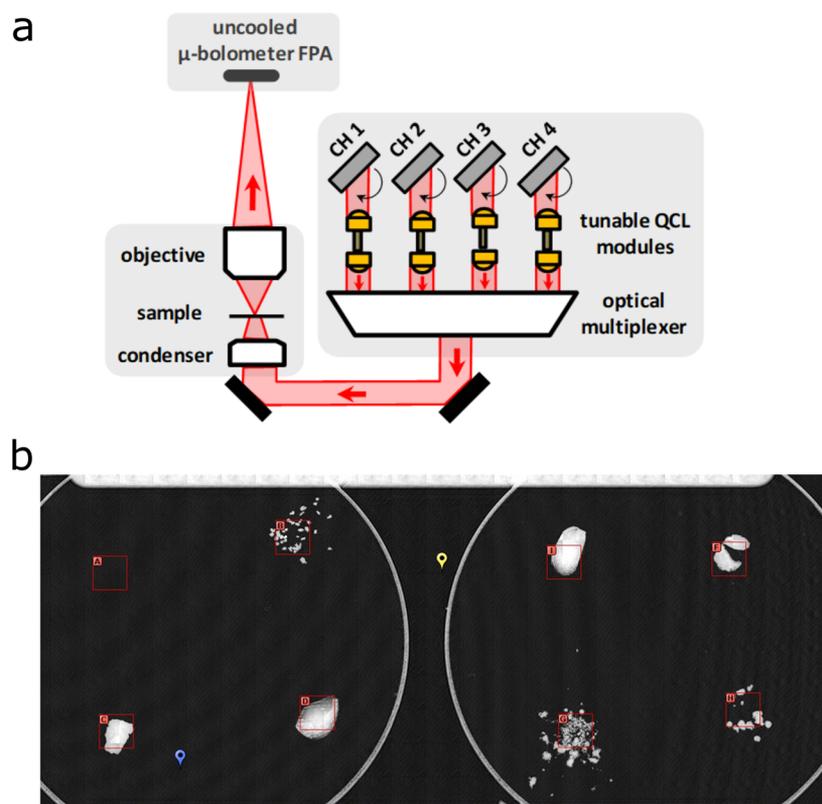
Figure 1. (a) Schematic overview of the beam path in the microscope from the quantum cascade laser (QCL) setup containing four laser chips (CH1 to CH4) measuring the sample in transmission before reaching the micro (μ) bolometer focal plane array (FPA) detector. (b) False-color image at 1470 cm^{-1} of the sample stage with reference materials placed on barium fluoride (BaF$_2$) windows (d = 25 mm) with selected (red squares) measurement fields.

images of large sample areas. Here, we report the development of a measurement routine for microplastics, allowing the data collection of up to 12 samples per working day (8 h). Subsampling for regions of interest on the filter area is also possible but, due to the throughput, not necessary anymore. The method was tested for measured areas of 12 × 12 mm^2 with a spatial pixel resolution from 4.2 μm down to 1.4 μm.

■ MATERIAL AND METHODS

QCL-IR Microscopy and Data Acquisition. The laser-based microscope SPERO QT (DRS Daylight Solutions) was equipped with an EC-QCL assembly of four different lasers covering the wavelength range from 1800 to 950 cm^{-1} following the general scheme, as depicted in Figure 1a. An FPA microbolometer with 480 × 480 pixels is used as detector. All measurements were performed via ChemVision, Version 3.2.6RC (DRS Daylight Solutions) software with 2 cm^{-1} spectral resolution. The system is equipped with a visible light lens and two IR objectives with 4× magnification (4.185 μm spatial resolution, 2 × 2 mm^2 field of view, LowMag) and 12.5× magnification (1.365 μm spatial resolution, 655 × 655 μm^2 field of view, HighMag). Both can be applied in reflection and transmission modes. Prior to a measurement series, the laser intensity/spectral range profile was calibrated for the optimal laser intensity and protection of the FPA microbolometer for window (barium fluoride (BaF$_2$), 2 mm thickness, d = 25 mm, Korth Kristalle) and filter (Anodisc, d = 25 mm, 0.2 μm, GE Whatman) materials. After calibration against the most limiting factor, the absorbance of the Anodisc filter, all further measurements were performed in the regions

from 1800 to 1184 and 1160 to 1084 cm^{-1} in transmission mode, taking 45 s for the pure measurement and about 15 s for data storage per measurement field.

QCL-Based Measurements for Single Polymers. To determine the ability of QCL to measure and differentiate polymers from each other, a total of 297 materials were measured using a single-field measurement with the LowMag objective. The instrument allows the definition of several regions of interest (ROIs) followed by an automated measurement in one manipulation step. Therefore, several particles (up to eight) were placed on the window. The operator took a monochromatic mosaic at a chosen wave-number (1470 cm^{-1}) over the whole slide (see Figure 1b). Each photo of the individual field of view took less than a second.

Afterward, ROIs were defined according to the position of the individual particles, named with the numerical ID within the reference database[26] and measured automatically. The resulting data files were stored in the MATLAB file format.

QCL-Based Measurements for Environmental Samples. The samples on the Anodisc stored from previous studies were placed onto a BaF$_2$ window and mounted on the sample holder of the microscope stage. The sample preparation is described in detail within the respective studies (treated wastewater,[27] marine surface water,[25] marine sediment,[9] and snow[8] samples). To define the ROI, an overview image was collected at 1470 cm^{-1} using the respective lens (LowMag or HighMag). Afterward, the hyperspectral measurement was performed covering the central area ROI of 12 × 12 mm^2 (36 fields) using the LowMag objective. The measurement took 36
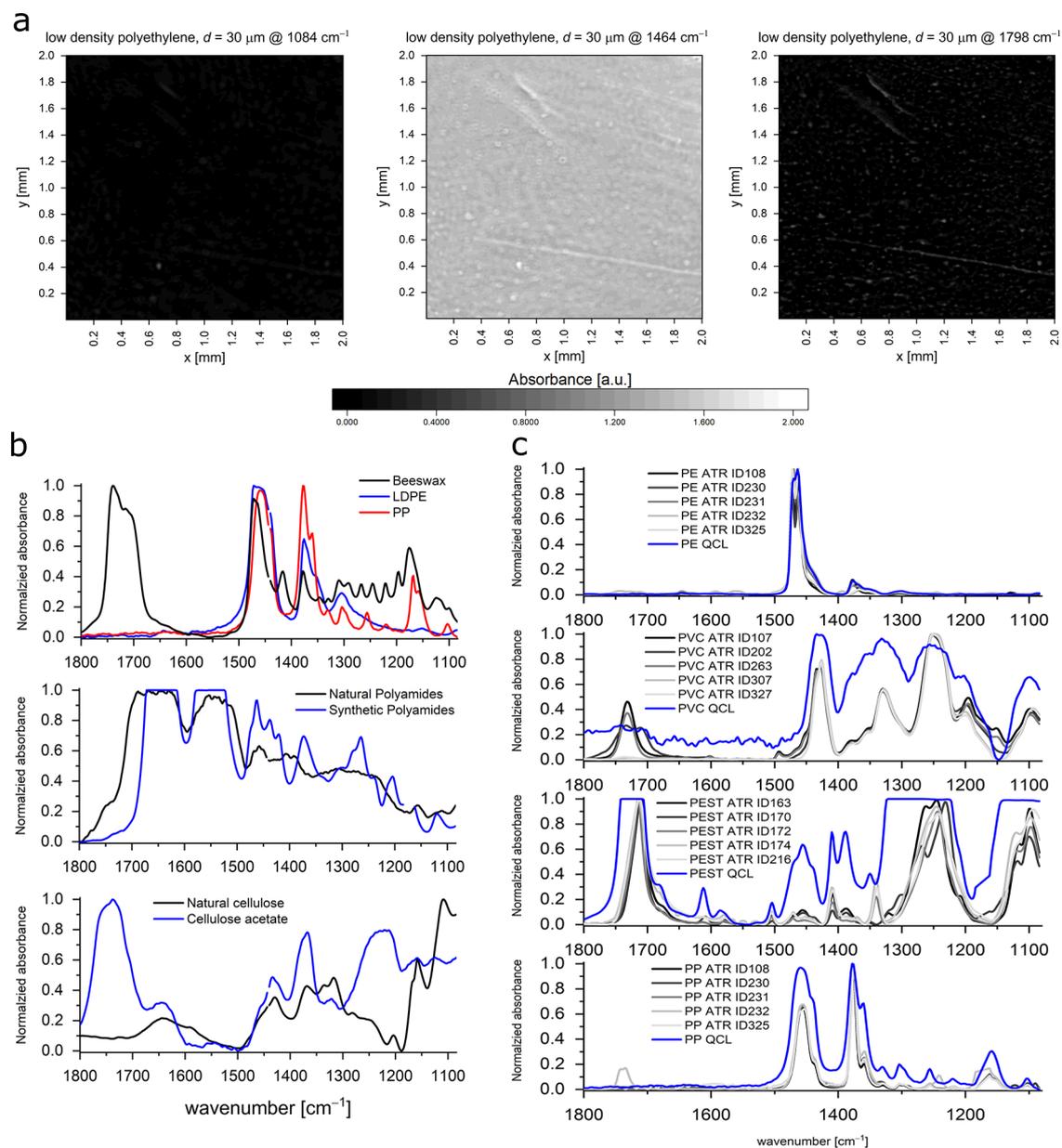
Figure 2. Application of external cavity quantum cascade laser (EC-QCL)-based hyperspectral imaging on the various reference polymers and comparison with attenuated total reflection (ATR) Fourier transform infrared (FT-IR) spectroscopy. (a) Absorbance signal at different wavenumbers of a polyethylene (PE) film, indicating impurities starting at 1700 cm^{-1}. (b) EC-QCL results in absorbance for three different interfering material groups: PE, polypropylene (PP), and natural bee waxes; natural and synthetic polyamides; and natural cellulose versus chemically modified one. (c) EC-QCL spectrum plotted against various spectra derived via ATR-FT-IR for the FT-IR database. Details of the materials (ID) can be found in the Supporting Information of Primpke et al.[26]

min and the resulting data files were stored in the MATLAB file format.

QCL-Based Measurements Using HighMag. Similar to LowMag, the sample on the Anodisc was placed onto a BaF$_2$ window, mounted on the sample holder of the microscope stage. Using HighMag, a ROI of 13.1 × 13.1 mm^2 (400 fields) was placed over the sample area and measured. The measurement took 347 min. As the generated data (92.1 million spectra) could not be visualized in OriginPro2017, the data set was reduced to a ROI of 12.4 × 12.4 mm^2 (361 fields), prior to data analysis via the Python script.

FT-IR Imaging Data. The data set RefEnv1 derived via FT-IR imaging data was chosen from our reference data set.[26] All measurement details are provided within the associated

study.[26] The data set was exported into the MATLAB file format via Bruker OPUS 7.5 (Bruker Optics GmbH, Ettlingen, Germany) using a custom-made macro (available upon request).

Hierarchical Cluster Analysis. The performed hierarchical cluster analysis was based on the procedure described in the literature.[26] First, the freely available attenuated total reflection (ATR)-FT-IR database,[26] containing $n = 326$ spectra of individual measured materials, was tested as a prescreening in the wavenumber region 1800−1084 cm^{-1}. To perform the process, the data set was reduced to the wavenumber regions 1800−1184 and 1160−1084 cm^{-1} (see the Supporting Information (SI) SI1.xlsx) and loaded into Primer 6 (PRIMER-e Ltd.). The resemblance based on the Hellinger

distance was calculated, and a hierarchical cluster analysis was performed. The obtained dendrogram was used as a support for the determination of polymer-type clusters, and each binning of spectra was manually confirmed by expert knowledge based on combined plots of the respective spectra of a cluster using OriginPro2017.

In total, 112 clusters (see SI1.xlsx and Figure S1) were determined, containing up to 27 spectra per cluster. The cluster ranking, data evaluation, and quality assurance were performed similarly to the FT-IR study, and a detailed description is provided in Paragraph S1 and Figure S2 in the Supporting Information. The final and quality-assured database is available as SI2.xslx. The working files for the Python script are combined in SI3.zip.

Identification and Quantification of Microplastics. Data analysis was performed via Python 3.7 using Spyder 4.1.1 on a computer equipped with an AMD Ryzen 3950x with 16 cores/32 threads at 3.6 GHz with 64 GB RAM and two SLI-bridged Nividia Windforce OC Geforce RTX2070 graphics cards using Samsung 970 SSDs as the hard drive for the calculations (1 TB, EVO) and the operating system (250 GB, EVO Plus). For analysis, the following Python packages were used: SimpleITK,[28−30] numpy, pandas, math, matplotlib, scipy.io,[31] time, and numba.cuda.[32]

Each variation of the database was tested using a specialized designed Python script. By utilizing the package Numba,[32] paralleled computing on normal desktop personal computers is possible, while a NVIDIA graphics card is mandatory to use this process via Compute Unified Device Architecture (CUDA). To achieve this goal, the previously applied[33] vector normalization and Pearson correlation were rewritten to be performed in a parallel computing manner. Using this type of calculation, the time demand for data analysis of 8 million spectra was reduced from several days to 6 h. Further, quality assurance performance was improved by saving the ID of the database together with x and y positions, hit quality index (HQI) g, and the polymer type p in one. csv file, avoiding large data sets of single files. The script is available in SI3.zip and will be updated in the future to increase the calculation performance.

To compare FT-IR imaging and EC-QCL imaging, the developed script was also used to analyze the respective FT-IR data. Here, the reference database[26] was applied. The number, polymer type, and size of the present MP were determined using APA[33] as a tool within Python for the EC-QCL data. Compared to the original study, the data output was improved by the mass calculation[34] using densities based on the material data sheets and literature works[35] (see Table S1). The determined FT-IR results were analyzed using APAv1.1.1.exe available at https://drive.google.com/drive/folders/1O3vtsb963KoGwsTTGvDZgo8KUqjGjNAD?usp=sharing as data handling within one Python script for both measurement methods could not be implemented yet.

To amend APA for EC-QCL, the particle gap closing mechanism (see Primpke et al.[33] for details) was improved by adding an additional filter. Here, the range check for potential pixels for closing was extended by a cross-hair-inspired shape, as depicted in Figure S3. Around the target pixel (shown in red) in the middle of the function, first, the closing of APA is performed (shown in green) and then the surrounding area was additionally checked for assigned pixels (shown in black). For this additional closing, the process was only performed if all pixels between the target pixel and the tested pixel were not

assigned to any polymer type. To further increase the performance, the closing procedure was modified away from SimpleITk using numpy tools instead.

All graphs and videos presented with measurement data were generated using OriginPro2017 and Inkscape 0.92, respectively. To investigate the individual wavenumbers, the single fields were merged within the Python script for absorbance at one wavenumber for the full map (see SI3.zip for the Python script) and exported as a text file for import into OriginPro2017. All other data was directly imported from the generated files of APA or calculated from these files using Microsoft Excel 2016.

■ RESULTS AND DISCUSSION

Database Generation and Cluster Validation. Current, state-of-the-art, FPA-based FT-IR microscopes cover a spectral range from 3600 to 900 cm^{-1}, while for EC-QCL-based systems, the range can be designed by the choice of laser chips during the manufacturing process. The investigated system had an interval from 1800 to 950 cm^{-1} available. Here, CH vibrations at ∼2750 to 3000 cm^{-1} and OH signals from 3200 to −3600 cm^{-1} are missing for the identification of microplastics. Interestingly, it was found that in contrast to the strong absorption below 1250 cm^{-1} for FT-IR of the most commonly used aluminum oxide filters[19] (Anodisc), EC-QCL enables investigation of samples on Anodisc filters down to 1084 cm^{-1} (with a small gap between 1160 and 1184 cm^{-1}), representing the lower limit for the following analyses. For region 1250−1084 cm^{-1}, we refer to an extended wavenumber range in the following.

In total, 289 polymers in fiber, pellet, powder, and sheet forms (see Figure 2a and SI4.avi using polyethylene (PE) as an example) were investigated for the successful separation of synthetic materials from natural ones in the region of 1800−1084 cm^{-1} (see Figure 2b). Up to seven polymers were placed on the BaF$_2$ window and measured together with the background within one measurement series.

It was found that all types of important synthetic polymers can be differentiated from known, interfering, and natural polymers like proteins (hereon termed natural polyamides), cellulose, and waxes. The spectra of polypropylene (PP) and low-density polyethylene (LDPE) showed major differences from those of beeswax. For LDPE, the peaks at 1800−1650 and 1180−1140 cm^{-1} exhibit a clear separation from beeswax. For PP, the separation of beeswax via FT-IR is easily possible by the peaks between 2750 and 3000 cm^{-1}, but for EC-QCL, they showed higher similarity. Still, both signals can be well separated because PP is missing the peak at 1800−1650 cm^{-1} and has a stronger absorbance at 1400−1340 cm^{-1}, while the peak at 1180−1140 cm^{-1} is present in both cases. Furthermore, several small peaks between 1200 and 1340 cm^{-1} are solely present for beeswax. For natural polyamides and synthetic polyamides, similar results were found (see Figure 2b). Both materials are strong IR absorbers so even thin films already lead to total absorption of amide I and amide II peaks, similar to FT-IR. Still, both materials can be well separated, as synthetic polyamides have a lower bandwidth of these peaks and more pronounced peaks in the region from 1500 to 1250 cm^{-1}.

By comparison with an existing attenuated total reflection (ATR)-FT-IR database, the results were further supported. The same sample materials were investigated using EC-QCL to achieve harmonized results with FT-IR studies (see Figure
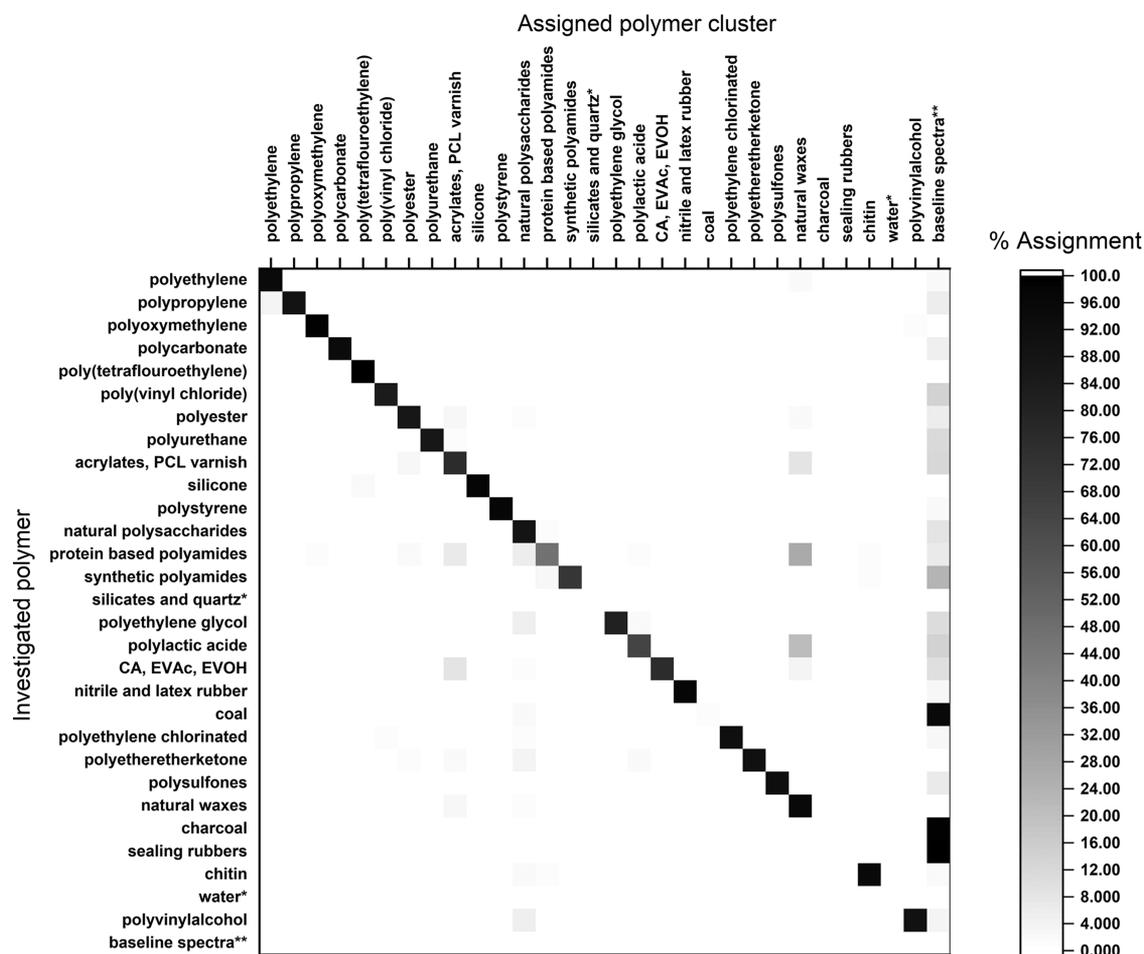
Figure 3. Cross validation of polymer types separable via external cavity quantum cascade laser (EC-QCL) based on the hierarchical cluster analysis of attenuated total reflection (ATR)-Fourier transform infrared (FT-IR) spectra with EC-QCL spectra added to the respective clusters excluding quartz and silicates and water. *No investigated material data available. ** To improve spectral assignment quality. CA, cellulose acetate; EVAc, ethylene-vinyl-acetate; EVOH, ethylene-vinyl-alcohol; and PCL, polycaprolactone.

2c). In general, all polymers showed the same peaks in EC-QCL as the respective ATR-FT-IR spectra. For poly(vinyl chloride) (PVC, Figure 2c), the presence/absence of plasticizers was also visible within this region by the peak at 1800−1650 cm^{-1} from CO groups of commonly used chemicals for the referenced ATR-FT-IR spectra. Simultaneously, a minor peak at around 1200 cm^{-1} was observed. Here, the extended wavenumber range for Anodisc filters may be beneficial to investigate and quantify plasticizers within PVC. Only for polyesters (PEST), a larger difference was found in the region of 1350−1200 cm^{-1} due to strong absorbance in transmission (see Figure 2c). Several other peaks were cutoff to a straight line due to total absorbance. It has to be highlighted that this linear cutoff is superior to FT-IR imaging, which normally still has strong noise at similar peaks.

To perform automated analysis, a hierarchical cluster analysis of the ATR-FT-IR data was performed similarly to FT-IR imaging. The derived results were manually evaluated and annotated to polymer-type clusters. Afterward, the database generated was further enhanced with EC-QCL spectra in the respective clusters. The final cross-correlation table is depicted in Figure 3.

The results showed that most materials were assigned to the correct clusters; however, acrylates, polycaprolactone, varnish (ACV), natural polysaccharides, and natural waxes were also assigned to materials originating from other polymer types. For natural polysaccharide assignments, this has to be expected as worn lab coats and other materials were made from cellulose (part of the cluster) and present on the BaF$_2$ windows as contamination. The strong assignment of natural waxes to natural polyamides could be assigned to one reference material. Here, a reference spectrum for the cluster calculation originated from beeswax and was assigned to natural polyamides. The wax was covered by a film similar to natural polyamides and measured via ATR-FT-IR. If measured in transmission by EC-QCL, the wax material has a much higher share on the determined spectrum, causing an assignment to the natural wax clusters. To avoid further confusion, this spectrum was removed from the final database. Samples of coal, charcoal, and sealing rubbers could not be assigned to their respective polymer types, only to baseline spectra, due to unsuitably thick material. Similar to FT-IR, these materials were also difficult to measure by EC-QCL.

Analysis of an FT-IR Reference Sample and Quality Assurance. The resulting database was evaluated via an environmental sediment sample, the reference sample RefEnv1.[26] The FT-IR imaging data sets were investigated using the Python script generated for EC-QCL for comparison of the results, and the analysis took 1 h. Compared to, and in agreement with, previous studies, the data showed a different
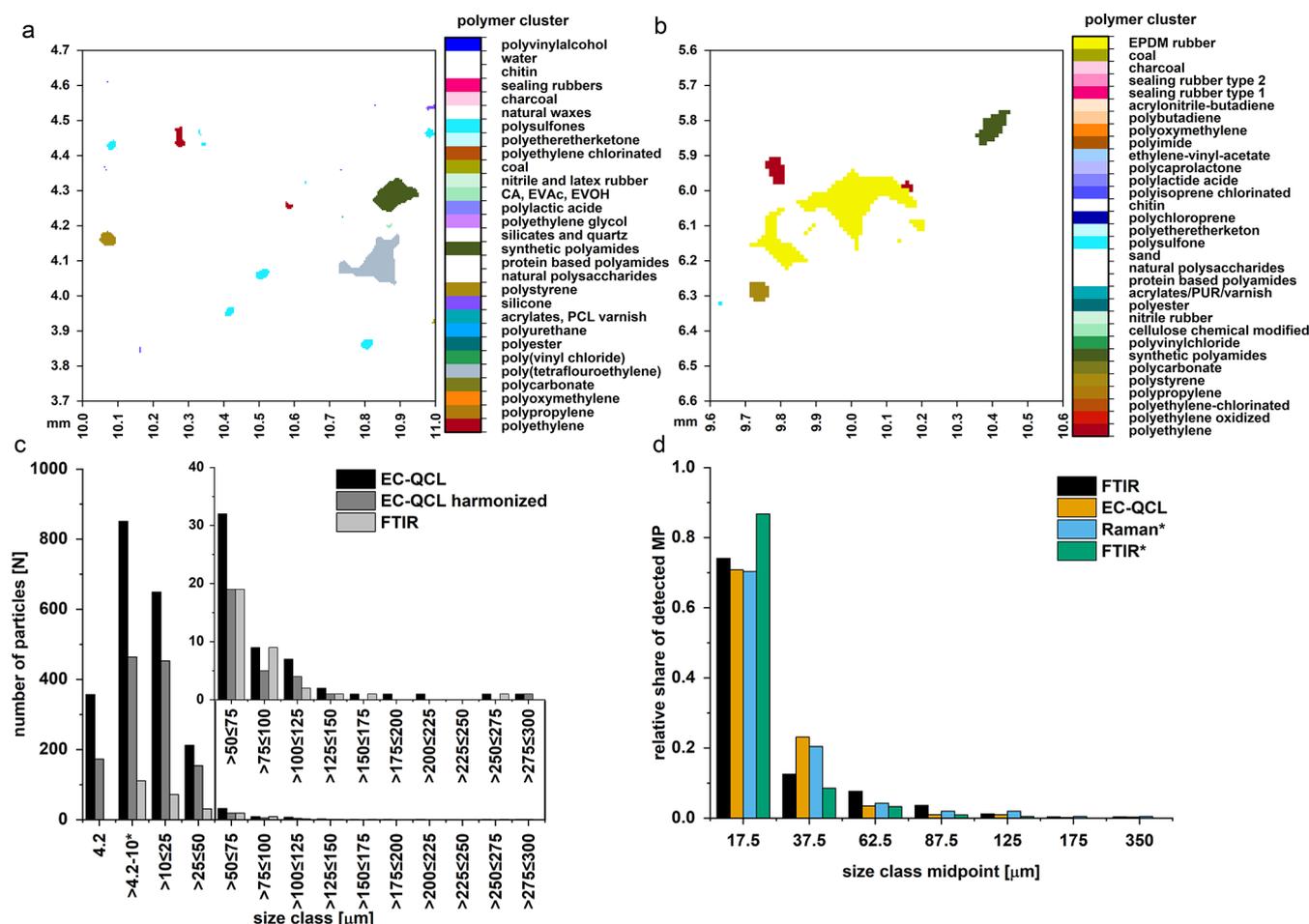
Figure 4. (a) Area on the filter representing the same set of particles for external cavity quantum cascade laser (EC-QCL) and (b) Fourier transform infrared (FT-IR) hyperspectral imaging based on the arrangement of the polyamide, polyethylene, and polystyrene particles (shifted by ~45° due to instrumental differences and sample placement). (c) Determined particle numbers in the different size classes of synthetic polymers for EC-QCL and FT-IR. To allow a better comparative investigation due to the extended wavenumber range for EC-QCL, its result was also harmonized to the cluster derived for FT-IR by excluding all clusters solely determinable for EC-QCL. (d) Comparison with other studies using automated single-particle exploring (ASPE) Raman microscopy[37] and hyperspectral FT-IR imaging on the same filter areas. * Data from the literature.[37] CA, cellulose acetate; EPDM, ethylene propylene diene monomer; EVAc, ethylene-vinyl-acetate; EVOH, ethylene-vinyl-alcohol; PCL, polycaprolactone; and PUR: polyurethane.

assignment rate only for the polymer-type ethylene propylene diene monomer (EPDM), similar to siMPle.[36] Analysis of the EC-QCL data took 6 h for eight times more spectra. Subsequently, data quality for EC-QCL was assured by a manual reanalysis of the assigned spectra for each individual polymer type. The derived minimum threshold values for positive identification are summarized in Table S1, along with a depiction of the analytical result for the whole sample surface (see Figure S4). In Figure 4a, a close-up view of a chosen area is shown together with the summarized results of both data sets.

The results of EC-QCL hyperspectral imaging showed a higher sensitivity toward plastic particles, which when compared to FT-IR imaging had a higher number and variability of particles assigned to polymer types (see Figure 4a). The yellow particles (EDPM) in the middle of the FT-IR image were not assigned by EC-QCL. After examining the visual image of the particle in question, an organic cellular structure was observed (data not shown), indicating a missed assignment for FT-IR imaging. In previous analyses, via Bruker OPUS[26] and siMPle,[36] this particle showed a less pronounced

assignment and a different shape. For FT-IR, the match is mainly driven by the CH signal between 2980 and 2780 cm^{-1}. Due to the smaller spectral range of the EC-QCL setup, this peak was excluded from the sample data and the spectrum was not assigned to any synthetic polymer type. In addition, the assigned PA (dark green) particle was larger and different in shape using EC-QCL. However, the assigned polystyrene (PS) particle appears to be smaller by EC-QCL, while poly(phenyl)-sulfone (PPSU) particles were easily identified by EC-QCL. While FT-IR only found one particle, EC-QCL determined eight particles present. Additionally, silicones and poly-(tetrafluoroethylene) (PTFE) could be detected on Anodisc filters by EC-QCL due to the extended wavenumber range, which are otherwise not measurable using FT-IR imaging systems. In total, the EC-QCL analysis found five times more particles, and importantly, those <10 μm (see Figure 4b) for the overall result. Moreover, an increased identification rate was also found for polymer types detectable by both methods (EC-QCL harmonized).

The study of Cabernard et al.[37] used a similar comparative approach via gold-coated PC membranes for FT-IR imaging
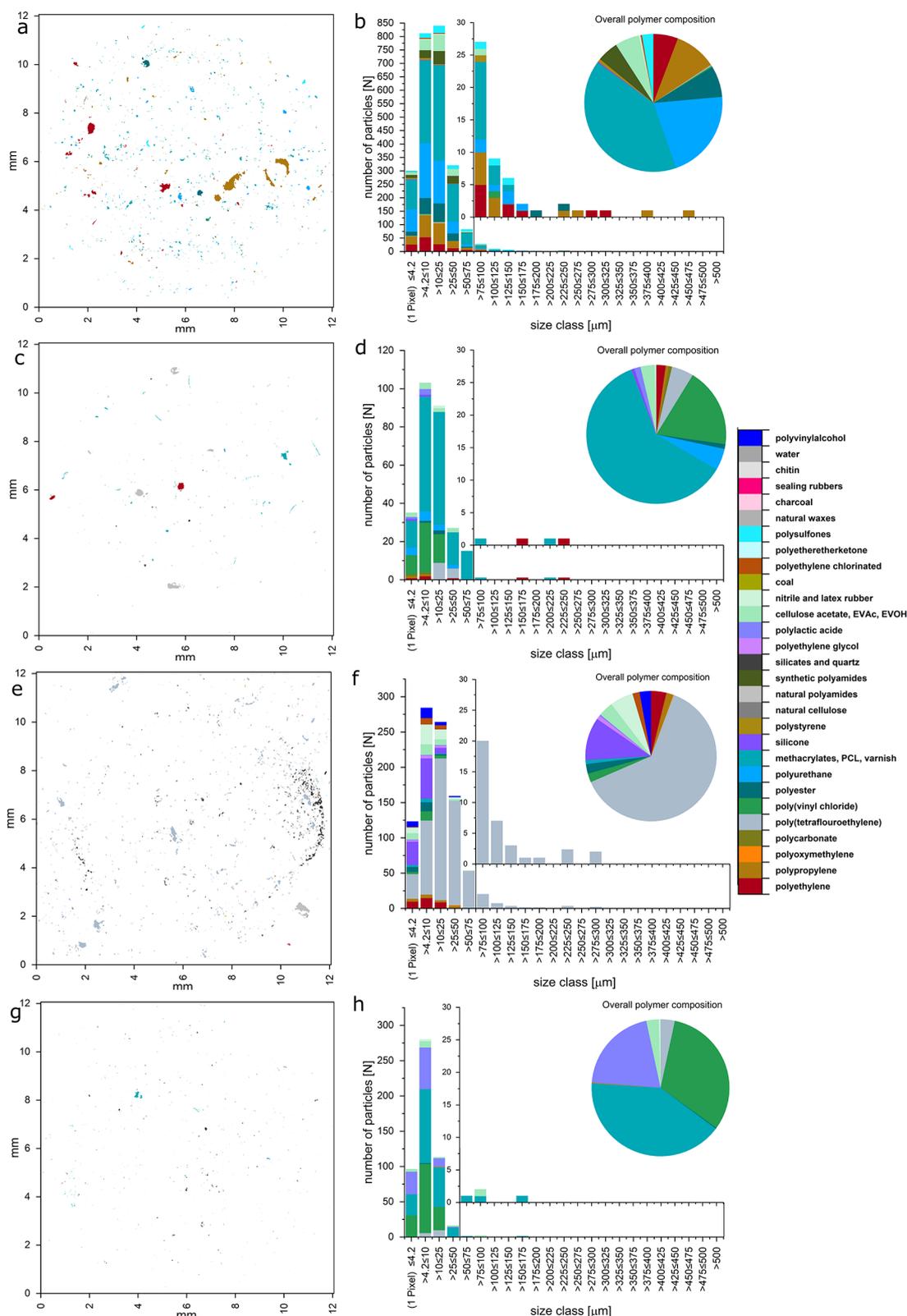
Figure 5. Exemplary analysis of Anodisc-filtered samples from different environmental matrices. (a, c, e, g) Polymer-dependent false-color images highlighting the detected materials ranging from synthetic to nonsynthetic types. (b, d, f, h) Identified synthetic polymer types are binned into size classes (area based) together with a zoom on the size fraction >75 μm with the exception >50 μm for melted snow. In addition, the polymer composition for the whole sample is depicted. The filters originate from previous studies on (a, b) treated wastewater,[27] (c, d) marine surface water,[25] (e, f) Arctic deep-sea sediment,[9] and (g, h) European snow samples.[8] For the Arctic deep-sea sediments, the signal of the polypropylene support ring of the Anodisc was removed prior to image analysis. A false-color image of untreated data is depicted in Figure S7a. The high numbers of poly(tetrafluoroethylene) for Arctic deep sea was confirmed as contamination by the separation device based on the analysis of the blank sample (see Figure S7b,c). PCL, polycaprolactone; EVAc, ethylene-vinyl-acetate; and EVOH, ethylene-vinyl-alcohol.

and automated single-particle exploring (ASPE) Raman microscopy. Even though identical regions could not be investigated in our study due to technical reasons, the full filter area with the majority of the particles was measured by both EC-QCL and FT-IR. In Figure 4d, a comparison of the determined relative share of the assigned particles with the size classification of Cabernard et al.[37] is depicted. Both FT-IR measurements show a similar trend with a sharp increase of particle numbers at the lowest size class (17.5 μm size class midpoint), while a lower number was determined at the 37.5 μm size class midpoint when comparing to Raman and EC-QCL measurements. These results based on the similar relative shares indicate an equal data quality of EC-QCL measurements compared to Raman measurements whereas Anodisc filters were used. With one complete measurement possible within 36 min, compared to several days or subsampling strategies necessary for Raman microscopy, EC-QCL shows promise for being an optimal candidate for routine or monitoring measurements.

The scope of the method was further tested on the second objective available (HighMag), which has a pixel resolution of 1.4 μm on the filter area (see Paragraph S2 for details and Figures S5 and S6). Here, the high potential to analyze particles <10 μm was found, while the measurement conditions itself need to be optimized in future studies.

Analysis of Selected Environmental Samples. Subsequently, LowMag was applied to three examples of purified samples from different environmental compartments (treated wastewater,[27] marine surface water,[25] and marine sediment[9] samples). These sample types have different levels of MP contamination. To further examine the limitations of the method, we added a melted snow sample,[8] which did not receive any purification and was directly filtered onto the Anodisc. The results are depicted as false-color images together with the determined particle sizes and polymer compositions in Figure 5.

Using EC-QCL, MPs were identified in all environmental compartments in agreement with the FT-IR measurements in the respective studies.[8,9,25,27] In general, the trend toward smaller particle sizes was confirmed. In contrast to FT-IR, where a single pixel had always the highest abundance of MP, the combination of the microbolometer FPA with an EC-QCL system determined a different trend. In three of the four samples, the highest number of MP was found in the second size class, which is close to the diffraction limit ~10 μm. While a few smaller particles could be detected, the result clearly shows that even with a lower pixel resolution on the FPA, the diffraction limit affects the analysis. Also, EC-QCL did not apply data binning, which is summing up spectra of several pixels into a combined spectrum representing a larger area, applied in most of the FT-IR studies.[9,25,27] Therefore, the data of single pixels should be taken with care if not excluded like in other studies[38] or were tested against binned measurements.[8] In the following discussion, these particles were not excluded due to the high similarity of the found polymer composition to the higher size classes. All particle data is additionally available in full details in SI5.zip as individual excel files.

Starting with the treated wastewater samples (Figure 5a,b), similar polymer types but larger numbers of particles were found (7212 N m^{-3} EC-QCL, 1250 N m^{-3} FT-IR). While the larger-sized particles were dominated by PE, PEST, and PP, particularly high numbers of the polymer-type ACV were found for smaller sized particles. In the original study, these

particles only had a minor contribution. In contrast, the presence of various PS types, which are binned in one polymer type in this study, could not be confirmed to a similar extent. Still, the high variability of polymer types was confirmed, yet the relative share of different polymer types changed. While the original measurement was based on a manual analysis of 25% of the filter area, leading to a slightly decreased level of comparability, the process using EC-QCL has a lower demand for the measurement and user time.

For the marine surface water sample (Figure 5c,d), similar numbers of particles (185 N m^{-3} EC-QCL, 245 N m^{-3} FT-IR) were found for blank-corrected data (see Figures S7 and S8). However, even after this correction, a lower share of PE and EPDM was found using EC-QCL, while higher numbers of PVC were found. While the large numbers of PVC are striking, similar results were also indicated in other studies. Hendrickson et al.[39] compared pyrolysis-GC/MS with ATR-FT-IR and found a similar result due to the chlorination of PE. This is further supported by a recent study comparing pyrolysis-GC/MS with FT-IR imaging on the exact same sample.[40] By the higher power of the EC-QCL system and the smaller wavenumber range, the sensitivity for PVC was increased, making it possible to identify compared to FT-IR imaging. The excluded $CH_{2/3}$ bands in the wavenumber region 3000−2700 cm^{-1} allow for a better library search, as the peaks in the region often drive the library search into the PE or EPDM cluster. Another factor may be the weathering status[41] of the polymers, as the applied library is currently missing these aged materials, and its impact will be investigated in the future.

In contrast, the deep-sea sediments (Figure 5e,f) from the Fram Strait showed an unexpectedly high level of plastic abundance with a high share to PTFE and silicone. In the original study, it was the sample with the lowest abundance[9] that was also confirmed in a follow-up study.[42] Nevertheless, when using FT-IR imaging with Anodiscs, PTFE and silicone cannot be detected. Due to this fact, both materials are used during sample preparation (e.g., in sealings and for squeeze bottles). To confirm sample contamination by these materials, the blank sample was investigated and similarly high numbers of PTFE were found. One major source of the contamination was found to be the ball valve of the microplastic sediment separator[43] due to the abrasion of the sealing material. During the density separation, this part of the apparatus is in permanent contact with the sample. By blank correction and exclusion of PTFE from the results (450 N kg (dw)$^{-1}$ EC-QCL, 67 N kg (dw)$^{-1}$ FT-IR), the level was still higher than that derived via FT-IR, but the polymer composition (see Figure S8b) contains similar polymers as those detected in the original study (PE-Cl, PP, PVC, PEST, and rubber type 2). From the EC-QCL analysis, additional materials like nitrile rubber, cellulose acetates, ACV, PCL, and PUR were found. A major contribution was particles <10 μm (328 N kg (dw)$^{-1}$) due to the higher sensitivity of EC-QCL for these sizes.

For the snow sample (Figure 5g,h), a similar result to that for the marine surface water sample was found using EC-QCL, with lower numbers of PE, PP, nitrile rubber, and EPDM detected and assignments to PVC and PLA, which were both not found via FT-IR. The total particle numbers also increased by a factor of eight (90 893 N L^{-1} EC-QCL, 11 786 N L^{-1} FT-IR). Similar to the deep-sea sediment sample, the difference was mainly driven by MP <10 μm (67 142 N L^{-1}). In comparison to the FT-IR study, the main polymer contribution switched from EPDM and nitrile rubber to ACV and PVC.

The exact cause for this change could not be determined, but similar implications to those for the marine surface water are to be expected as the main reason for this difference and will be targeted in future studies.

Application of EC-QCL in Monitoring of MP. With EC-QCL-based hyperspectral infrared imaging, the measurement speed can be accelerated to a level suitable for daily laboratory routine schedules and time slots. Compared to FT-IR imaging, the expenditure of time is around ten times lower per measurement. By applying defined ROIs (e.g., 12×12 mm^2 areas), the measurement time is fixed, which is essential for routinely monitoring microplastics in environmental, food, and animal feed samples.

Most materials identified by FT-IR were also detected with the EC-QCL-based system. Following quality assurance, a similar level of confidence was achieved while allowing a larger number of samples to be processed. Due to the application of EC-QCL laser as a light source and its smaller wavenumber range, similar, if not better, data quality for polymer type and particle number could be achieved. Still, especially for samples with small particles, the currently used database may overlook weathered particles to a higher extent compared to FT-IR while having a higher sensitivity for others (e.g., PVC and PPSU). This issue will be addressed by a database update covering a clustering of various wavenumber regions for the different systems available.

Furthermore, measuring large areas spectrally without preselecting regions of interest gives access to the complete data of the sample, allowing for measurement verification and contamination tracing by operators or sample preparation.

The design of the analysis approach allows the separation between measurement and data analysis. While one measurement can be collected within 40 min depending on the ROI, the data analysis (library search, annotation of materials, size of particles, etc.) can be performed on a separate personal computer. Here, we used the provided Python script and in addition improved the free software tool siMPle[36] to read in this data, which will be made available in a future update. With the use of siMPle, a user-friendly solution will be provided, allowing rapid quality assurance and control of the spectral data. In conclusion, the application of EC-QCL measurements in combination with the derived data analysis allows, for the first time, the rapid identification and quantification of microplastics, without the necessity of subsampling or other technical solutions, yet yielding the highest level of data quality.

■ ASSOCIATED CONTENT

ⓈＩ Supporting Information

The Supporting Information is available free of charge at https://pubs.acs.org/doi/10.1021/acs.est.0c05722.

> Dendrogram derived based on the Hellinger distance and manual evaluation; cluster analysis and data validation; cross validation of polymer types separable with the range 1800−1084 cm^{-1} by ATR-FTIR data; area around a target pixel investigated for closing; minimum thresholds for the hit quality index; polymer-type-dependent false-color overview images of the sample surface of RefEnv1; detailed results high resolution (HighMag) hyperspectral imaging; sample RefEnv1 measured with EC-QCL at a magnification of 12.5; polymer numbers derived from the sample

RefEnv1 using LowMag and HiMag; false-color overview images of the Arctic deep-sea sediment sample and the analysis results of procedural blank samples; and synthetic polymers identified in marine surface water and deep-sea sediments (PDF)

Input data and results of the cluster analysis (XLSX)

Database in Excel format in the wavenumber regions 1800−1184 and 1160−1084 cm^{-1} (XLSX)

Python scripts and databases used in this study (ZIP)

Exemplary video of the measurement results for polyethylene in the region of 1800−1084 cm^{-1} (MPG)

All measurement result used in this study (ZIP)

■ AUTHOR INFORMATION

Corresponding Author

Sebastian Primpke − *Alfred Wegener Institute Helmholtz Centre for Polar and Marine Research, Biologische Anstalt Helgoland, 27498 Helgoland, Germany;* ⓞ orcid.org/0000-0001-7633-8524; Email: sebastian.primpke@awi.de

Authors

Matthias Godejohann − *MG Optical Solutions GmbH, 86919 Utting/Ammersee, Germany*

Gunnar Gerdts − *Alfred Wegener Institute Helmholtz Centre for Polar and Marine Research, Biologische Anstalt Helgoland, 27498 Helgoland, Germany*

Complete contact information is available at:
https://pubs.acs.org/10.1021/acs.est.0c05722

Author Contributions

S.P. contributed to the experimental design, Python code, data analysis, and data visualization and wrote the manuscript with the contribution of all authors. M.G. contributed to the measurements, experimental design, and data analysis. G.G. contributed to the conception of the experiment as well as to the design and data analysis.

Notes

The authors declare the following competing financial interest(s): Sebastian Primpke and Gunnar Gerdts are free of competing interests. Matthias Godejohann has to report competing interests: Matthias Godejohann is owner of MG Optical Solutions GmbH, which is selling and technically supporting the microscopes in a selected number of countries in Europe, such as Austria, Germany, Nordic countries and Switzerland.

■ ACKNOWLEDGMENTS

■ REFERENCES

(1) Hartmann, N. B.; Huffer, T.; Thompson, R. C.; Hassellov, M.; Verschoor, A.; Daugaard, A. E.; Rist, S.; Karlsson, T.; Brennholt, N.; Cole, M.; Herrling, M. P.; Hess, M. C.; Ivleva, N. P.; Lusher, A. L.; Wagner, M. Are We Speaking the Same Language? Recommendations for a Definition and Categorization Framework for Plastic Debris. *Environ. Sci. Technol.* **2019**, *53*, 1039−1047.

(2) Ajith, N.; Arumugam, S.; Parthasarathy, S.; Manupoori, S.; Janakiraman, S. Global distribution of microplastics and its impact on marine environment—a review. *Environ. Sci. Pollut. Res.* **2020**, *27*, 25970−25986.

(3) Kögel, T.; Bjorøy, Ø.; Toto, B.; Bienfait, A. M.; Sanden, M. Micro- and nanoplastic toxicity on aquatic life: Determining factors. *Sci. Total Environ.* **2020**, *709*, No. 136050.

(4) Kirstein, I. V.; Kirmizi, S.; Wichels, A.; Garin-Fernandez, A.; Erler, R.; Löder, M.; Gerdts, G. Dangerous hitchhikers? Evidence for potentially pathogenic Vibrio spp. on microplastic particles. *Mar. Environ. Res.* **2016**, *120*, 1−8.

(5) Kanhai, L. D. K.; Gardfeldt, K.; Krumpen, T.; Thompson, R. C.; O'Connor, I. Microplastics in sea ice and seawater beneath ice floes from the Arctic Ocean. *Sci. Rep.* **2020**, *10*, No. 5004.

(6) Peeken, I.; Primpke, S.; Beyer, B.; Gutermann, J.; Katlein, C.; Krumpen, T.; Bergmann, M.; Hehemann, L.; Gerdts, G. Arctic sea ice is an important temporal sink and means of transport for microplastic. *Nat. Commun.* **2018**, *9*, No. 1505.

(7) Suaria, G.; Perold, V.; Lee, J. R.; Lebouard, F.; Aliani, S.; Ryan, P. G. Floating macro- and microplastics around the Southern Ocean: Results from the Antarctic Circumnavigation Expedition. *Environ. Int.* **2020**, *136*, No. 105494.

(8) Bergmann, M.; Mützel, S.; Primpke, S.; Tekman, M. B.; Trachsel, J.; Gerdts, G. White and wonderful? Microplastics prevail in snow from the Alps to the Arctic. *Sci. Adv.* **2019**, *5*, No. eaax1157.

(9) Bergmann, M.; Wirzberger, V.; Krumpen, T.; Lorenz, C.; Primpke, S.; Tekman, M. B.; Gerdts, G. High Quantities of Microplastic in Arctic Deep-Sea Sediments from the HAUSGARTEN Observatory. *Environ. Sci. Technol.* **2017**, *51*, 11000−11010.

(10) Allen, S.; Allen, D.; Phoenix, V. R.; Le Roux, G.; Durántez Jiménez, P.; Simonneau, A.; Binet, S.; Galop, D. Atmospheric transport and deposition of microplastics in a remote mountain catchment. *Nat. Geosci.* **2019**, *12*, 339−344.

(11) GESAMP. *Guidelines for the Monitoring and Assessment of Plastic Litter in the Ocean*; 2019; p 123.

(12) Triebskorn, R.; Braunbeck, T.; Grummt, T.; Hanslik, L.; Huppertsberg, S.; Jekel, M.; Knepper, T. P.; Krais, S.; Müller, Y. K.; Pittroff, M.; Ruhl, A. S.; Schmieg, H.; Schür, C.; Strobel, C.; Wagner, M.; Zumbülte, N.; Köhler, H.-R. Relevance of nano- and microplastics for freshwater ecosystems: A critical review. *TrAC, Trends Anal. Chem.* **2019**, *110*, 375−392.

(13) Primpke, S.; A. Dias, P.; Gerdts, G. Automated identification and quantification of microfibres and microplastics. *Anal. Methods* **2019**, *11*, 2138−2147.

(14) Liu, F.; Olesen, K. B.; Borregaard, A. R.; Vollertsen, J. Microplastics in urban and highway stormwater retention ponds. *Sci. Total Environ.* **2019**, *671*, 992−1000.

(15) Vianello, A.; Jensen, R. L.; Liu, L.; Vollertsen, J. Simulating human exposure to indoor airborne microplastics using a Breathing Thermal Manikin. *Sci. Rep.* **2019**, *9*, No. 8670.

(16) Schwaferts, C.; Niessner, R.; Elsner, M.; Ivleva, N. P. Methods for the analysis of submicrometer- and nanoplastic particles in the environment. *TrAC, Trends Anal. Chem.* **2019**, *112*, 52−65.

(17) Anger, P. M.; von der Esch, E.; Baumann, T.; Elsner, M.; Niessner, R.; Ivleva, N. P. Raman microspectroscopy as a tool for microplastic particle analysis. *TrAC, Trends Anal. Chem.* **2018**, *109*, 214−226.

(18) Zarfl, C. Promising techniques and open challenges for microplastic identification and quantification in environmental matrices. *Anal. Bioanal. Chem.* **2019**, *411*, 3743−3756.

(19) Primpke, S.; Christiansen, S. H.; Cowger, W.; De Frond, H.; Deshpande, A.; Fischer, M.; Holland, E. B.; Meyns, M.; O'Donnell, B.

A.; Ossmann, B. E.; Pittroff, M.; Sarau, G.; Scholz-Bottcher, B. M.; Wiggin, K. J. Critical Assessment of Analytical Methods for the Harmonized and Cost-Efficient Analysis of Microplastics. *Appl. Spectrosc.* **2020**, *74*, 1012−1047.

(20) Renner, G.; Schmidt, T. C.; Schram, J. Analytical methodologies for monitoring micro(nano)plastics: Which are fit for purpose? *Curr. Opin. Environ. Sci. Health* **2018**, *1*, 55−61.

(21) Dümichen, E.; Eisentraut, P.; Bannick, C. G.; Barthel, A. K.; Senz, R.; Braun, U. Fast identification of microplastics in complex environmental samples by a thermal degradation method. *Chemosphere* **2017**, *174*, 572−584.

(22) Fischer, M.; Scholz-Böttcher, B. M. Microplastics analysis in environmental samples − recent pyrolysis-gas chromatography-mass spectrometry method improvements to increase the reliability of mass-related data. *Anal. Methods* **2019**, *11*, 2489−2497.

(23) Kuepper, C.; Kallenbach-Thieltges, A.; Juette, H.; Tannapfel, A.; Großerueschkamp, F.; Gerwert, K. Quantum Cascade Laser-Based Infrared Microscopy for Label-Free and Automated Cancer Classification in Tissue Sections. *Sci. Rep.* **2018**, *8*, No. 7717.

(24) Barroso Pena, A.; Ketelhut, S.; Godejohann, M.; Kemper, B.; Schnekenburger, J. *Optical Imaging Methods for Label Free Detection of Microplastics in Cells, Tissues and Environmental Organisms (Conference Presentation)*; SPIE, 2020, Vol. 11243.

(25) Lorenz, C.; Roscher, L.; Meyer, M. S.; Hildebrandt, L.; Prume, J.; Löder, M. G. J.; Primpke, S.; Gerdts, G. Spatial distribution of microplastics in sediments and surface waters of the southern North Sea. *Environ. Pollut.* **2019**, *252*, 1719−1729.

(26) Primpke, S.; Wirth, M.; Lorenz, C.; Gerdts, G. Reference database design for the automated analysis of microplastic samples based on Fourier transform infrared (FTIR) spectroscopy. *Anal. Bioanal. Chem.* **2018**, *410*, 5131−5141.

(27) Mintenig, S. M.; Int-Veen, I.; Löder, M. G. J.; Primpke, S.; Gerdts, G. Identification of microplastic in effluents of waste water treatment plants using focal plane array-based micro-Fourier-transform infrared imaging. *Water Res.* **2017**, *108*, 365−372.

(28) Lowekamp, B. C.; Chen, D. T.; Ibanez, L.; Blezek, D. The Design of SimpleITK. *Front. Neuroinf.* **2013**, *7*, No. 45.

(29) Lehmann, G. Label object representation and manipulation with ITK. *Insight J.* **2007**, *8*, 1−31.

(30) Yoo, T. S.; Ackerman, M. J.; Lorensen, W. E.; Schroeder, W.; Chalana, V.; Aylward, S.; Metaxas, D.; Whitaker, R. Engineering and Algorithm Design for an Image Processing API: A Technical Report on ITK - the Insight Toolkit. In *Medicine Meets Virtual Reality 02/10*; Westwood, J. D.; Hoffman, H. M.; Robb, R. A.; Stredney, D., Eds.; IOS Press: Amsterdam, 2002; pp 586−592.

(31) Virtanen, P.; Gommers, R.; Oliphant, T. E.; Haberland, M.; Reddy, T.; Cournapeau, D.; Burovski, E.; Peterson, P.; Weckesser, W.; Bright, J.; van der Walt, S. J.; Brett, M.; Wilson, J.; Millman, K. J.; Mayorov, N.; Nelson, A. R. J.; Jones, E.; Kern, R.; Larson, E.; Carey, C. J.; Polat, İ.; Feng, Y.; Moore, E. W.; VanderPlas, J.; Laxalde, D.; Perktold, J.; Cimrman, R.; Henriksen, I.; Quintero, E. A.; Harris, C. R.; Archibald, A. M.; Ribeiro, A. H.; Pedregosa, F.; van Mulbregt, P.; Vijaykumar, A.; Bardelli, A. P.; Rothberg, A.; Hilboll, A.; Kloeckner, A.; Scopatz, A.; Lee, A.; Rokem, A.; Woods, C. N.; Fulton, C.; Masson, C.; Häggström, C.; Fitzgerald, C.; Nicholson, D. A.; Hagen, D. R.; Pasechnik, D. V.; Olivetti, E.; Martin, E.; Wieser, E.; Silva, F.; Lenders, F.; Wilhelm, F.; Young, G.; Price, G. A.; Ingold, G.-L.; Allen, G. E.; Lee, G. R.; Audren, H.; Probst, I.; Dietrich, J. P.; Silterra, J.; Webber, J. T.; Slavič, J.; Nothman, J.; Buchner, J.; Kulick, J.; Schönberger, J. L.; de Miranda Cardoso, J. V.; Reimer, J.; Harrington, J.; Rodríguez, J. L. C.; Nunez-Iglesias, J.; Kuczynski, J.; Tritz, K.; Thoma, M.; Newville, M.; Kümmerer, M.; Bolingbroke, M.; Tartre, M.; Pak, M.; Smith, N. J.; Nowaczyk, N.; Shebanov, N.; Pavlyk, O.; Brodtkorb, P. A.; Lee, P.; McGibbon, R. T.; Feldbauer, R.; Lewis, S.; Tygier, S.; Sievert, S.; Vigna, S.; Peterson, S.; More, S.; Pudlik, T.; Oshima, T.; Pingel, T. J.; Robitaille, T. P.; Spura, T.; Jones, T. R.; Cera, T.; Leslie, T.; Zito, T.; Krauss, T.; Upadhyay, U.; Halchenko, Y. O.; Vázquez-Baeza, Y.; SciPy, C. SciPy 1.0: fundamental algorithms for scientific computing in Python. *Nat. Methods* **2020**, *17*, 261−272.

(32) Lam, S. K.; Pitrou, A.; Seibert, S. In *Numba: a LLVM-Based Python JIT Compiler*, In Proceedings of the Second Workshop on the LLVM Compiler Infrastructure in HPC; Association for Computing Machinery: Austin, Texas, 2015; p Article 7.

(33) Primpke, S.; Lorenz, C.; Rascher-Friesenhausen, R.; Gerdts, G. An automated approach for microplastics analysis using focal plane array (FPA) FTIR microscopy and image analysis. *Anal. Methods* **2017**, *9*, 1499−1511.

(34) Simon, M.; van Alst, N.; Vollertsen, J. Quantification of microplastic mass and removal rates at wastewater treatment plants applying Focal Plane Array (FPA)-based Fourier Transform Infrared (FT-IR) imaging. *Water Res.* **2018**, *142*, 1−9.

(35) *Polymer Data Handbook*, 2nd ed.;Mark, J. E., Ed.; Oxford University Press: New York, 2009.

(36) Primpke, S.; Cross, R. K.; Mintenig, S. M.; Simon, M.; Vianello, A.; Gerdts, G.; Vollertsen, J. Toward the Systematic Identification of Microplastics in the Environment: Evaluation of a New Independent Software Tool (siMPle) for Spectroscopic Analysis. *Appl. Spectrosc.* **2020**, *74*, 1127−1138.

(37) Cabernard, L.; Roscher, L.; Lorenz, C.; Gerdts, G.; Primpke, S. Comparison of Raman and Fourier Transform Infrared Spectroscopy for the Quantification of Microplastics in the Aquatic Environment. *Environ. Sci. Technol.* **2018**, *52*, 13279−13288.

(38) Liu, F.; Vianello, A.; Vollertsen, J. Retention of microplastics in sediments of urban and highway stormwater retention ponds. *Environ. Pollut.* **2019**, *255*, No. 113335.

(39) Hendrickson, E.; Minor, E. C.; Schreiner, K. Microplastic Abundance and Composition in Western Lake Superior As Determined via Microscopy, Pyr-GC/MS, and FTIR. *Environ. Sci. Technol.* **2018**, *52*, 1787−1796.

(40) Primpke, S.; Fischer, M.; Lorenz, C.; Gerdts, G.; Scholz-Böttcher, B. M. Comparison of pyrolysis gas chromatography/mass spectrometry and hyperspectral FTIR imaging spectroscopy for the analysis of microplastics. *Anal. Bioanal. Chem.* **2020**, *412*, 8283−8298.

(41) Andrady, A. L. The plastic in microplastics: A review. *Mar. Pollut. Bull.* **2017**, *119*, 12−22.

(42) Tekman, M. B.; Wekerle, C.; Lorenz, C.; Primpke, S.; Hasemann, C.; Gerdts, G.; Bergmann, M. Tying up Loose Ends of Microplastic Pollution in the Arctic: Distribution from the Sea Surface through the Water Column to Deep-Sea Sediments at the HAUSGARTEN Observatory. *Environ. Sci. Technol.* **2020**, *54*, 4079−4090.

(43) Imhof, H. K.; Schmid, J.; Niessner, R.; Ivleva, N. P.; Laforsch, C. A novel, highly efficient method for the separation and quantification of plastic particles in sediments of aquatic environments. *Limnol. Oceanogr.: Methods* **2012**, *10*, 524−537.